NeuroImage: Clinical 11 (2016) 388–397

Contents lists available at ScienceDirect

NeuroImage: Clinical

journal homepage: www.elsevier.com/locate/ynicl

A brain stress test: Cerebral perfusion during memory encoding in mild cognitive impairment

Long Xie[a,f,*], Sudipto Dolui[b,d,e], Sandhitsu R. Das[a,e], Grace E. Stockbower[c,d], Molly Daffner[c,d], Hengyi Rao[b,d], Paul A. Yushkevich[a,e], John A. Detre[b,d,e], David A. Wolk[c,d]

[a]Penn Image Computing and Science Laboratory (PICSL), Department of Radiology, University of Pennsylvania, Philadelphia, PA, USA
[b]Center for Functional Neuroimaging, Department of Neurology, Department of Radiology, University of Pennsylvania, Philadelphia, PA, USA
[c]Penn Memory Center, University of Pennsylvania, Philadelphia, PA, USA
[d]Department of Neurology, University of Pennsylvania, Philadelphia, PA, USA
[e]Department of Radiology, University of Pennsylvania, Philadelphia, PA, USA
[f]Department of Bioengineering, University of Pennsylvania, Philadelphia, PA, USA

ARTICLE INFO

Article history:
Received 21 July 2015
Received in revised form 16 February 2016
Accepted 1 March 2016
Available online 2 March 2016

Keywords:
Alzheimer's disease
Arterial spin labeling
Biomarker
Medial temporal lobe
Scene-encoding memory task

ABSTRACT

Arterial spin labeled perfusion magnetic resonance imaging (ASL MRI) provides non-invasive quantification of cerebral blood flow, which can be used as a biomarker of brain function due to the tight coupling between cerebral blood flow (CBF) and brain metabolism. A growing body of literature suggests that regional CBF is altered in neurodegenerative diseases. Here we examined ASL MRI CBF in subjects with amnestic mild cognitive impairment (n = 65) and cognitively normal healthy controls (n = 62), both at rest and during performance of a memory-encoding task. As compared to rest, task-enhanced ASL MRI improved group discrimination, which supports the notion that physiologic measures during a cognitive challenge, or "stress test", may increase the ability to detect subtle functional changes in early disease stages. Further, logistic regression analysis demonstrated that ASL MRI and concomitantly acquired structural MRI provide complementary information of disease status. The current findings support the potential utility of task-enhanced ASL MRI as a biomarker in early Alzheimer's disease.

1. Introduction

Over 5 million people in the United States carry a diagnosis of Alzheimer's disease (AD) and this number will rise to 13.5 million by the year 2050 due to our aging demography (Thies and Bleiler, 2013). The search for disease modifying medications, which halt or delay progression, remains the central goal of AD research. It is generally accepted that interventions are likely to be most effective early in the disease course when symptoms are minimal, if present at all. As such, a parallel endeavor has been the development of biomarkers that are sensitive to the early manifestations of the disease and its treatment.

While considerable progress has been made in the development of biomarkers that are sensitive to the molecular pathology of AD [e.g. CSF (cerebrospinal fluid) Aβ/tau amyloid PET], these measures appear to be less sensitive to clinical status and disease progression (Engler et al., 2006; Jack et al., 2008, 2009, 2010; Jagust et al., 2009, 2010; Vemuri et al., 2009a, 2009b). Measures that are able to track progression in the early stages of disease would be particularly valuable as outcome measures in clinical trials and, eventually, clinical practice.

Measures of brain structure (e.g. volumetric MRI) and function [e.g. flourodeoyglucose positron emission tomography (FDG PET)] have been conceptualized as markers of the 'downstream' effects of the molecular pathology of AD and are thought to reflect neurodegeneration. Consistent with this notion, changes detected with these modalities tend to more closely parallel disease progression and clinical phenotype (Jack et al., 2009, 2010; Jagust et al., 2009; Vemuri et al., 2009b). FDG PET may be particularly sensitive to the early consequences of the AD pathologic process. A theoretical basis for this claim is that the glucose metabolism measured by this modality is largely a reflection of synaptic activity (Schwartz et al., 1979; Attwell and Laughlin, 2001). These synaptic changes are thought to precede neuronal death and are possibly mediated, in part, by soluble Aβ (Walsh and Selkoe, 2004); whereas the structural changes measured by MRI are dependent on neuronal

Abbreviations: AAL, Anatomical Automatic Labeling; ASL, arterial spin labeled; aCBF, absolute cerebral blood flow; a-MCI, amnestic mild cognitive impairment; BOLD, blood oxygen level dependent; CBF, cerebral blood flow; CSF, cerebrospinal fluid; FDG PET, flourodeoyglucose positron emission tomography; FWER, familywise error rate; HC, health control; MCI, mild cognitive impairment; MMSE, mini-mental status exam; MNI, Montreal Neurological Institute; MTL, medial temporal lobe; PASL, pulsed ASL; pCASL, pseudo-continuous ASL; PCC, posterior cingulate cortex; ROI, region of interest; rCBF, relative cerebral blood flow; SCORE, structural correlation based outlier rejection.

* Corresponding author at: Penn Image Computing and Science Laboratory (PICSL), 3700 Hamilton Walk, Richard Building, 6th Floor, Philadelphia, PA 19104, USA.
E-mail address: lxie@seas.upenn.edu (L. Xie).

http://dx.doi.org/10.1016/j.nicl.2016.03.002

and neuropil degeneration. Further, the sensitivity of FDG PET to synaptic function makes it well-positioned to track disease course, as synapse loss appears to be the best correlate of cognitive function relative to other pathologic markers (Terry et al., 1991).

Arterial spin labeled perfusion MRI (ASL MRI) provides a quantitative measure of regional cerebral blood flow (CBF), which is generally thought to be tightly coupled to regional brain metabolism (Raichle, 1998). ASL MRI uses magnetically labeled arterial blood water as an endogenous 'tracer' for blood flow. CBF can be reliably quantified in absolute terms (Alsop et al., 2010), and has been validated against 15-O PET CBF (Ye et al., 2000; Xu et al., 2010; Zhang et al., 2014). While the information obtained from this modality is likely to overlap with the information yielded from FDG PET, ASL MRI has the advantages of being less expensive, less invasive, and easily acquired during routine MRI scans. Moreover, in addition to resting state ASL MRI, short task-related sequences can be easily implemented during scans, potentially providing more sensitive functional information.

Prior investigations have assessed resting state ASL MRI in neurodegenerative populations (Xu et al., 2007; Alsop et al., 2008; Chao et al., 2009; Dai et al., 2009; Chen et al., 2011; Wang et al., 2013). Several studies in patients with AD have found areas of hypoperfusion which have been broadly consistent with the parietotemporal pattern of hypometabolism shown in the FDG PET literature (Alsop et al., 2000, 2010; Dai et al., 2009; Yoshiura et al., 2009; Hu et al., 2010; Chen et al., 2011). A more limited number of ASL MRI studies of patients with amnestic mild cognitive impairment (a-MCI), a group commonly conceptualized as enriched in patients with the early clinical changes of AD (Petersen et al., 2009), have produced similar findings (Xu et al., 2007; Chao et al., 2009; Dai et al., 2009; Zhang et al., 2011).

Perfusion changes in medial temporal lobes (MTL) in AD and a-MCI have been inconsistent. Bangen et al. (2012) reported decreased perfusion in MTL among a-MCI patients, parallel to studies of FDG PET that have found MTL hypometabolism (Minoshima et al., 1997; De Santi et al., 2001; Mevel et al., 2007; Chételat et al., 2008; Mosconi et al., 2008). On the other hand, there have also been a few reports of hyper-perfusion in the MTL of patients with AD and a-MCI (Alsop et al., 2008; Dai et al., 2009) after correcting for underlying atrophy. This finding resonates with work utilizing blood oxygen level dependent functional MRI (BOLD fMRI), which has also found MTL hyperactivation in a-MCI relative to cognitively normal adults (Dickerson and Sperling, 2009; Yassa et al., 2010; Das et al., 2013). However, the increased MTL recruitment reported in these BOLD fMRI studies have been in the context of active memory encoding relative to control conditions with the exception of the Das et al. study which described increased MTL subregion connectivity at rest.

Task-related measurements of brain function may increase sensitivity for detecting regional alterations in brain function by requiring activation of specific networks that may be dysfunctional, resulting in accentuation of group differences. Additionally, task performance may simply minimize variation of subjects` brain activity relative to unconstrained resting stated to thereby enhance discrimination between populations. This may be particularly true for the case of MTL activation, since these structures may be engaged in resting states (Stark and Squire, 2001). Only one prior study has analogously examined task-related ASL measurements relative to rest in a-MCI (Xu et al., 2007). That study reported that CBF during task accentuated discrimination between a-MCI and healthy control groups, but only included a relatively small cohort (12 a-MCI patients).

To further assess the value of both rest and task-related CBF for distinguishing a-MCI from normal aging, the current study compared CBF measured by ASL in patients with a-MCI and cognitively normal healthy controls (HC), both at rest and during performance of a scene-encoding memory task previously demonstrated to be associated with modulation of MTL function (Fernández-Seara et al., 2007; Mechanic-Hamilton et al., 2009). To measure CBF, we employed pseudo-continuous ASL (pCASL), which appears to have significant signal-to-noise and test-retest reliability advantages relative to the more widely available pulsed ASL (PASL) used in most prior studies of these populations (Wu et al., 2009; Chen et al., 2010). We predicted that task-related CBF would accentuate group differences relative to ASL measured at rest and that these differences would likely be most prominent in MTL structures, as a reflection of the task and the clinical population. We were particularly interested in determining whether CBF measures were increased or decreased in a-MCI given prior inconsistencies in the literature.

2. Materials and methods

2.1. Participants

Sixty-five patients with a-MCI [age: 74.0 ± 6.2 (standard deviation) years; education: 15.8 ± 3.0 (standard deviation) years; 24 female] and 62 HC subjects [age: 70.5 ± 8.8 (standard deviation) years; education: 16.6 ± 2.7 (standard deviation) years; 39 female] participated in the study. All participants were recruited from the Penn Memory Center, a National Institute of Aging supported Alzheimer`s disease center and a memory disorders specialty clinic. As part of their evaluation at the Penn Memory Center, each patient and HC participant underwent an extensive evaluation, including medical history and physical examination, neurological history and examination, and psychometric assessment. All patients had at least the following neuropsychological measures: Mini-Mental Status Exam (MMSE) (Folstein et al., 1975); Digit Span subtest of the Wechsler Adult Intelligence Scale III (Wechsler, 1987); Category fluency (animals) (Spreen and Strauss, 1998); Consortium to Establish a Registry for AD Word List Memory test (Morris et al., 1989); Trail Making Tests A and B (Reitan, 1958); and a 30-item version of the Boston Naming Test (Kaplan et al., 1983). Additionally, relevant blood work and brain imaging studies were evaluated. Clinical diagnosis was determined by review of the above data at a consensus conference attended by neurologists, neuropsychologists, and psychiatrists.

Diagnosis of amnestic MCI was made following the criteria outlined by Petersen and others (Petersen, 2004; Winblad et al., 2004; Petersen et al., 2009). Patients had to have a memory problem, generally intact cognitive functioning and activities of daily living, objective evidence of memory impairment on cognitive testing, and not qualify for a diagnosis of dementia. There was no strict cut-off for the degree of memory impairment, but generally these patients performed greater than 1.5 standard deviations below our age-adjusted means on verbal and/or non-verbal memory tests. Rather than a strict cut-off, clinical judgment accounting for the premorbid status of the patient and performance on other cognitive tests weighs into decisions of objective impairment (Petersen, 2004). Controls were defined by an absence of significant cognitive complaints, normal performance on age-adjusted cognitive measures, and consensus conference designation as 'normal.' Inclusion criteria included age between 50 and 85, >7 years education, and English speaking at an early age. Participants were excluded if they had a history of clinical stroke, significant traumatic brain injury, alcohol or drug abuse/dependence, prior electroconvulsive therapy, and any significant disease or medical/psychiatric condition that was felt to impact neuropsychological performance. The study was approved by the Institutional Review Board of the University of Pennsylvania.

2.2. Scene-encoding memory task

A ~6 minute visual scene-encoding task was administered during ASL MRI scanning, as has been previously described (Fernández-Seara et al., 2007; Mechanic-Hamilton et al., 2009). The task involved the presentation of 72 complex visual scenes selected from a Photodisc (PhotoDisc, Inc., Seattle, WA, USA) photographic archive of real-world scenes. Pictures were presented as three blocks of 24 pictures each. Participants were instructed to try to remember these visual scenes for a

later memory test. To enhance the likelihood of 'deep' semantic encoding, subjects were instructed to make a subjective judgment as to whether or not the picture was meaningful to them and respond by button press. Interposed were three short 'rest' blocks in which an unrecognizable, pixelated image was repeated six times. A shaded 'X' or 'T' was embedded in these images at random location on the screen and subjects had to indicate which letter they observed. All images were presented for 3500 ms with a 500 ms interstimulus interval. A brief practice session was performed prior to entering the scanner. The behavioral task paradigm was implemented in E-prime (Psychology Software Tools, Pittsburgh, PA, USA) running on a PC laptop. In-scanner responses were made using a fiberoptic response system (FORP, Current Designs, Philadelphia, PA, USA). Images were back-projected onto a Mylar screen that the subject viewed through a mirror mounted on the head coil.

The task was performed as the last sequence of the scanning session and was followed immediately by a recognition memory test outside of the scanner. 40 visual scenes (20 studied; 20 unstudied) were presented on a laptop. Participants were instructed to make an 'old/new' decision depending on whether or not they thought the item had been previously studied. This assessment was self-paced. To account for false alarms to non-studied items, we derived a measure of discriminability, d-prime (d′), which was calculated in a standard fashion based on classic signal detection theory (Snodgrass and Corwin, 1988). Additionally, because d′ is undefined when either proportion is 0 or 1, we used standard formulas to convert these values: Hits = (#Hits + 0.5) / (#studied items + 1) and FA = (#FA + 0.5) / (#unstudied items + 1). Due to experimenter error in collection of recognition memory data, 16 subjects (4 HC and 12 a-MCI) could not be analyzed.

2.3. MRI acquisition

All imaging was performed on a 3T Siemens Trio MRI scanner (Erlangen, Germany) equipped with either a product eight-channel or thirty-two-channel array coil. High-resolution structural images were acquired with 3D-MPRAGE (Mugler and Brookeman, 1990) at 1 mm^3 isotropic resolution (TI = 950 ms, TE = 3 ms, TR = 1620 ms). A pCASL sequence (Wu et al., 2007; Dai et al., 2008) was used for the perfusion scans and was acquired using 2D gradient-echo echo planar imaging (GR-EPI). Imaging parameters included: TR/TE/FA = 4 s/19 ms/90°, 6 mm slice thickness, 1 mm inter-slice gap, 16 slices acquired in ascending order, 3.5 × 3.5 × 7 mm^3 resolution. Arterial spin labeling was implemented with mean Gz of 0.6 mT/m and 1640 Hanning window shaped RF pulses for a total labeling duration of 1.5s (RF duration 500 μs with 360 μs gap in between). The labeling plane was positioned 80 or 90 mm below the center of the imaging region and post-labeling delay was set to 1.5 s. All participants were scanned during a 'rest' and 'task' sequence, each sequence lasts ~6 min. Since scanning protocol changed during the course of the study (32 HC and 27 a-MCI scans were acquired with the original protocol and 34 HC and 35 a-MCI were acquired with the subsequent protocol), the number of pairs of interleaved label and control images for each sequence is variable. On average, 48 pairs were acquired for signal averaging. Due to technical issues or subject fatigue, 'task' scans for three subjects were cut short (only 37, 37 and 29 pairs were acquired, but the data quality was sufficient for inclusion in the study) and nine participants' 'task' scans (4 HC and 5 a-MCI) were not acquired.

2.4. Image processing and analysis

2.4.1. CBF quantification

ASL data processing and analyses were carried out with Statistical Parametric Mapping software (SPM8, Wellcome Department of Cognitive Neurology, UK) implemented in MATLAB 2013a (Math Works, Natick, MA) and FSL (http://www.fmrib.ox.ac.uk/fsl/). In house SPM add-on scripts (ASLtbx, available at http://www.cfn.upenn.edu/perfusion/software.htm, (Wang et al., 2008)) were used to quantify CBF values and reconstruct CBF maps for perfusion analysis. For each subject, ASL time series data were realigned to correct for head motion, co-registered with the anatomical image and smoothed in space using a three-dimensional, 4 mm full width at half maximum Gaussian kernel. The perfusion-weighted image series were then generated by pair-wise subtraction of the label and control images, followed by conversion to an absolute CBF image series based on a modified single compartment continuous ASL perfusion model (Wang et al., 2003).

Gray matter, white matter, and CSF probability maps for each subject were generated from the anatomical images. The high-resolution structural images were first subsampled to the resolution of the functional images. Then, tissue segmentation algorithm provided in SPM8 was used to generate the gray matter, white matter and CSF probability maps for the subsampled structural images.

In order to remove motion-degraded ASL MRI data and increase the reliability of CBF maps, the CBF image series were de-noised using a Structural Correlation based Outlier REjection (SCORE) algorithm. First, CBF pairs, whose mean gray matter CBF is not within physiologically possible range of [0, 150] (ml/100 g tissue/min), are discarded. Then, the pair that is most correlated (Pearson Correlation) with the current mean CBF image, estimated by using the remaining CBF image series, is iteratively removed. The stopping criteria for the iterative process are as follows: (1) only one CBF image left; or (2) the weighted CBF variance within the three tissue types (weighted by number of voxels of each tissue type) between successive iteration increases. SCORE is based on the assumption that the variance of the mean estimation should decrease when outlier pairs are removed, but increase when non-outlier pairs are removed. As such, when removal of the most correlated pair to the mean decreases variance, this suggests that this pair was disproportionately contributing to the mean and likely associated with artifact. Fig. 1 shows a detailed procedure of the SCORE algorithm.

The "cleaned" CBF maps were then normalized to 2 × 2 × 2 mm^3 Montreal Neurological Institute (MNI) template in a two-step manner: (1) a group-specific template were generated using the iterative unbiased template building algorithm (Avants et al., 2008) from all the anatomical images; (2) the template was then registered to the MNI standard space using ANTS deformable registration (Avants et al., 2008). With these two transformations, each cleaned CBF image was normalized to MNI space for statistical analysis.

For each subject, one rest CBF image and one task CBF image (if available) were generated. All the CBF images went through a final visual inspection for quality control. CBF images with non-physiological negative CBF clusters in gray matter, indicating MRI artifacts or instability of spin labeling, were excluded from the study.

In order to correct for global perfusion variations between different subjects, relative CBF (rCBF) images were also generated. The rCBF map of each subject was generated by dividing the CBF map by the average CBF within gray matter and white matter voxels. For clarity, we will refer to the original CBF maps as absolute CBF (aCBF).

2.4.2. Normalized hippocampal volume

To provide context to any observed group effects with ASL, we also measured hippocampal volume, a well-established biomarker for AD and a-MCI, derived from the anatomical image of each subject using the multi-atlas label fusion technique described in Wang et al. (2012). To correct for whole brain volume variability between subjects, intracranial volume, computed from brain mask (generated using FSL BET tool), was used to normalize hippocampal volume by applying the following equation:

$$\text{Normalized hippocampal volume} = \frac{\text{Mean ICV of all the subjects} \times \text{Hippocampal volume}}{\text{Subject's ICV}}.$$

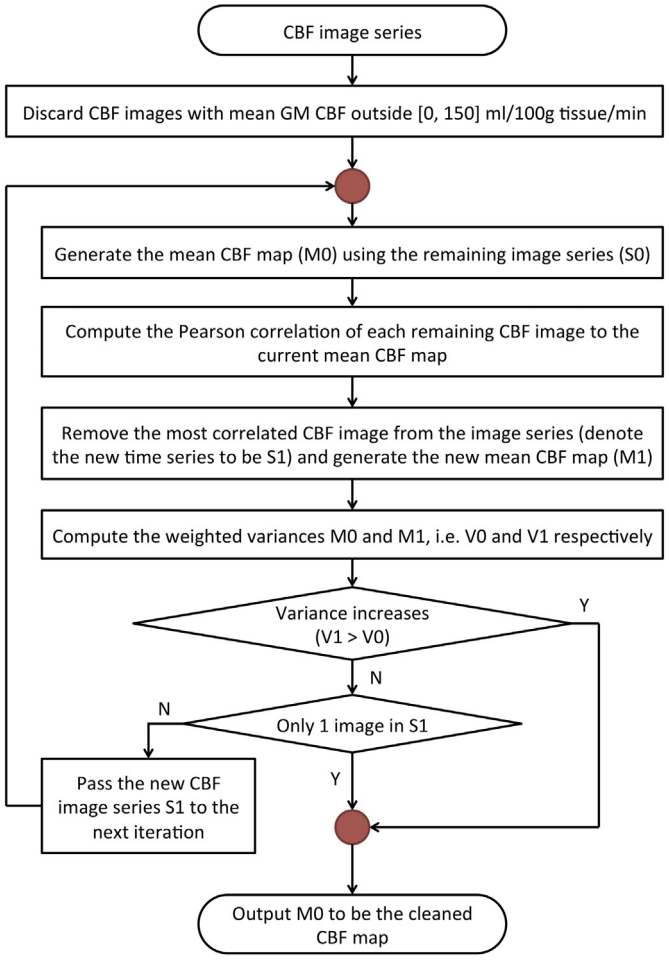

Fig. 1. A flow chart for the Structural Correlation based Outlier REjection (SCORE) algorithm.

2.4.3. Statistical analysis

The normalized CBF maps were entered into the whole brain voxel-wise general linear modeling analysis using the SPM8 PET model. For the direct comparisons at rest or task between the two groups, Analysis of Covariance (ANCOVA) was performed on the rCBF maps with age, gender and education as covariates. Paired *t*-tests were conducted to examine the task-induced CBF changes (task vs. rest) in HC and a-MCI groups using the aCBF maps. Note that aCBF was used here given that differences in global CBF is mitigated by the within subject comparison. Task activation differences between HC and a-MCI groups were examined using ANCOVA on the aCBF difference maps (task aCBF − rest aCBF) with age, gender and education as covariates as well. The parametric maps were enhanced by threshold-free cluster enhancement (Smith and Nichols, 2009) using the "randomize" package (Winkler et al., 2014). 10,000 permutations were run to convert the maps to voxel-wise p-value (both uncorrected and corrected for whole brain multiple comparison). Areas of activation were identified at a significance level of whole brain corrected $p < 0.05$ and cluster size larger than 20. A more liberal threshold of uncorrected $p < 0.001$ or $p < 0.01$ with cluster size larger than 20 voxels was applied to explore regional activation or CBF differences that did not survive the corrected threshold.

In addition to voxel-wise analysis, quantitative Region of Interest (ROI) analyses were performed to explore CBF changes at regions of interest. The ROIs were extracted from the Anatomical Automatic Labeling (AAL) template (Tzourio-Mazoyer et al., 2002), which included posterior cingulate cortex (PCC), precuneus, hippocampus and parahippocampal gyrus from both sides of the brain. Parietal and MTL ROIs were chosen because they have consistently been reported to be affected early in AD at rest in PET and other ASL studies (Petrie et al., 2009; Filippini et al., 2011). MTL regions were included in light of prior reports of either hypo- or hyper-perfusion associated with MCI/ AD and the fact that performance on the task (scene memory task) is likely dependent on these regions. All of these regions often associated with memory and default mode network. Each ROI`s mean CBF values of the left and right hemispheres were averaged. In addition, quantitative ROI analysis was also performed using a functionally defined ROI based on the between group voxel-wise rCBF difference map at scene-encoding task (HC > a-MCI, $p < 0.01$ after correcting for whole-brain multiple comparisons). Similar to the whole brain voxel-wise analyses, ANCOVA was applied to examine the between group effects (using rCBF) with age, gender and education as covariates. A 2 (groups: HC, a-MCI) × 2 (conditions: rest, task) mixed-effects ANOVA with these covariates, was conducted to look at the interaction between group and condition (using aCBF) and within group effects.

ANCOVA was also used to test the between group effects of normalized hippocampal volume with age, gender and education as covariates. To investigate whether normalized hippocampal volume and ASL measurements provide independent information concerning disease status, a two-level hierarchical logistic regression analysis was performed. Age, gender and education entered the model in the first step as fixed variables. Normalized hippocampal volume and mean relative CBF of all the ROIs from AAL template (including rest and task rCBF) were included in a step-wise manner (forward conditional step-wise) in the second step of the model. Noted that the functionally defined ROI was excluded from the model, which is because the ROI was defined post hoc. It wouldn't be appropriate to include the functionally defined ROI in the logistic regression analysis.

Comparisons of psychometric and demographic were determined by contingency χ^2 test (gender) or two-sample *t*-test (the other items). All statistical analyses were two-sided. Corrections for multiple comparisons were done using familywise error rate (FWER). The above statistical analyses were performed using standard methods in SPSS 20.0 (Chicago, IL).

3. Results

3.1. Psychometric and demographic data

Demographic and psychometric data for the a-MCI and HC groups are shown in Table 1. Age of the a-MCI patients was significantly higher than HC group ($t_{125} = 2.6$, $p < 0.05$), but there was no significant difference in education ($t_{125} = 1.6$, $p > 0.1$). There are significantly more

Table 1
Demographic and neuropsychological data.

	a-MCI (n = 65)	HC (n = 62)
Age	74.0* (6.2)	70.5 (8.8)
Education	15.8 (3.0)	16.6 (2.7)
Female:male	24:41**	39:23
MMSE	27.4** (1.7)	29.2 (1.0)
Trails A (seconds)	40.9** (22.7)	30.6 (10.8)
Trails B (seconds)	130.9** (72.5)	71.1 (29.6)
Digits forwards max[a]	8.6 (2.0)	9.1 (1.9)
Digits backwards max[a]	6.5** (2.0)	7.7 (2.3)
10-item word list immediate recall	16.8** (4.4)	23.4 (3.8)
10-item word list delayed recall	3.7** (2.0)	8.0 (2.0)
Category fluency (animals)	16.1** (5.2)	22.7 (5.3)
Boston naming test total	26.6** (3.1)	28.5 (1.7)
Scene recognition memory (d')[b]	1.56** (0.81)	2.30 (0.80)

Note: Standard deviations are in parentheses. * = $p < 0.05$, ** = $p < 0.01$, compared with the HC, tested by contingency χ^2 test (gender) or two-sample *t*-test (the other items).

[a] 5 a-MCI patients and 2 HC subject did not have Digits Forwards and Digits Backwards data available.

[b] 12 a-MCI patients and 4 HC subjects did not have Scene Recognition Memory data available.

males present in the a-MCI group ($\chi^2_1 = 8.6$, $p < 0.005$). The a-MCI group demonstrated significantly poorer Mini Mental Status Examination (MMSE; $t_{125} = 7.5$, $p < 0.001$). As expected, the groups also differed on a number of psychometric measures with a-MCI patients performing particularly poorly on tests of episodic memory. However, other cognitive domains were also impaired consistent with the fact that our a-MCI category included both single and multiple domain participants.

Recognition memory on the test phase of the scene-encoding task also significantly differed between the two groups with the a-MCI group displaying poorer discrimination ($t_{109} = 4.8$, $p < 0.001$). Nonetheless, patients with a-MCI were far from floor on the task and this performance was consistent with their overall memory function. Thus, it is unlikely that any difference between the groups on the task-related ASL measures was due primarily to differences in effort.

3.2. Neuroimaging data

10 out of 127 rest baseline CBF maps and 11 out of 118 task CBF maps were excluded from the analysis because of inadequate image quality. The number of remaining CBF measurements was 117 (59 HC and 58 a-MCI) for rest and 107 (55 HC and 52 a-MCI) for task. 103 subjects (53 HC and 50 a-MCI) had adequate rest and task CBF maps allowing for task activation analyses. The 3D glass brain and selected slices in the figures were generated using MRIcroGL (http://www.mccauslandcenter.sc.edu/mricrogl/) and ITK-SNAP (http://www.itksnap.org/pmwiki/pmwiki.php, (Yushkevich et al., 2006)).

3.2.1. CBF differences during rest baseline

We directly compared regional CBF differences between groups in the rest condition using a liberal threshold of $p < 0.001$ (uncorrected). Compared to HC, a-MCI patients displayed reduced rCBF in the bilateral

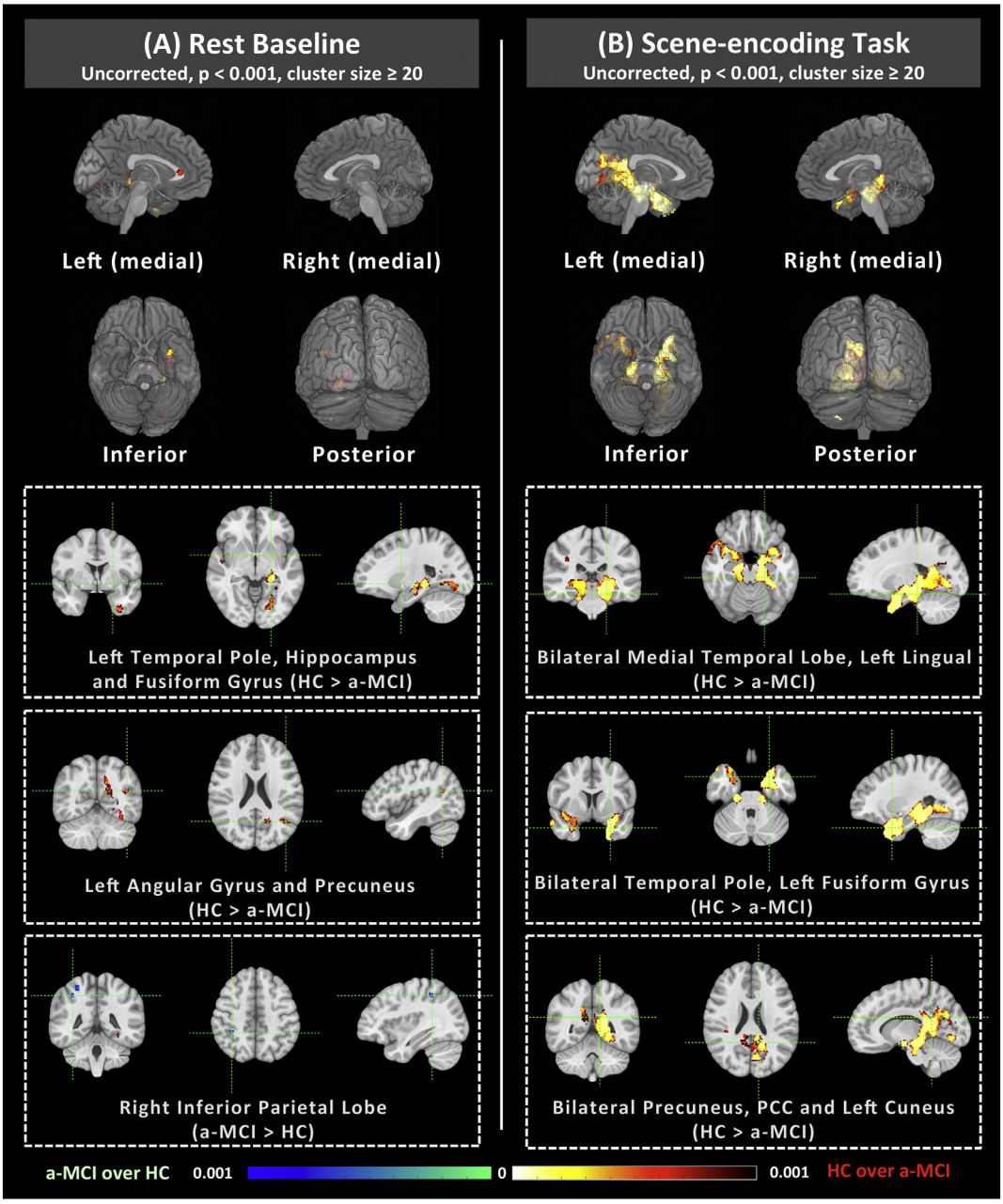

Fig. 2. Between group rCBF difference maps (A) at rest baseline and (B) at scene-encoding task. The figure shows that scene-encoding task accentuates functional abnormality. The effects are shown in 3D glass brain (top) and selected slices (bottom).

anterior cingulate cortex, left precuneus, left angular gyrus, left hippocampus, left fusiform gyrus and left temporal pole whereas HC demonstrated reduced rCBF in the right inferior parietal lobe (Fig. 2A). None of these effects survived after correcting for whole brain multiple comparisons.

3.2.2. CBF differences during scene-encoding task

Because CBF is a quantitative measure, we can directly compare regional CBF differences between groups during task without reference to baseline or other condition. Note that this type of comparison is not available in functional MRI made using BOLD measurements. Using the same threshold of $p < 0.001$ (uncorrected) (Fig. 2B), we found group differences between the a-MCI patients and HC that were much more extensive during task than rest, with a-MCI patients displaying reduced rCBF in multiple areas, including bilateral medial temporal lobes, bilateral temporal pole, bilateral precuneus/PCC, left lingual gyrus, left fusiform gyrus, left cuneus, and left superior occipital lobe. These effects appeared greater in the left hemisphere than in the right hemisphere. Indeed, most of the left hemisphere clusters remained significant after correcting for multiple comparisons (Fig. 3).

3.2.3. Task versus rest CBF differences

We also measured task activation in reference to rest CBF maps. As shown in Fig. 4A, robust activations were found in the bilateral visual cortex, bilateral fusiform gyrus, bilateral parahippocampal gyrus, cerebellum, bilateral parietal lobe and right frontal lobe in the HC group. The pattern for the a-MCI patients was similar (Fig. 4B) except for stronger frontal activation (including additional recruitment of bilateral insula, left frontal lobe) and weaker partial lobe activation, as well as MTL effects (including no activations in bilateral MTL and left parietal lobe). A direct comparison of task versus rest activation difference between groups is displayed in Fig. 4C. Using a liberal uncorrected threshold of $p < 0.01$, we found higher HC task activation in bilateral MTL, right inferior temporal gyrus and higher activation at bilateral anterior cingulate gyrus, right superior temporal gyrus in a-MCI.

3.2.4. ROI analysis of CBF and hippocampal volume

As displayed in Fig. 5, measurements of rCBF in a priori ROI's, HC displayed significantly greater rCBF in the hippocampus ($F_{1,112} = 8.9$, $p < 0.01$) during rest than a-MCI. Similarly, using the functionally defined ROI, defined as the FWER-corrected cluster (HC > a-MCI, $p < 0.01$) that discriminated groups in the task condition, HC's had higher rCBF than a-MCI patients in this region also at rest ($F_{1,112} = 7.5$, $p < 0.01$). On the other hand, during task, a-MCI patients displayed significantly decreased perfusion in PCC ($F_{1,102} = 10.1$, $p < 0.01$), hippocampus ($F_{1,102} = 23.0$, $p < 0.001$), parahippocampal gyrus ($F_{1,102} = 19.7$, $p < 0.001$) and in the functionally defined ROI ($F_{1,102} = 33.9$, $p < 0.001$) than HC. ANOVA showed that task activation of HC was significantly higher than a-MCI in parahippocampal gyrus ($F_{1,98} = 4.8$, $p < 0.05$) and functionally defined ROI ($F_{1,98} = 9.2$, $p < 0.005$). In follow-up paired *t*-tests, parahippocampal gyrus ($t_{52} = 2.7$, $p < 0.01$) and functionally defined ROI ($t_{52} = 2.5$, $p < 0.05$) showed significantly higher mean task aCBF than rest aCBF in HC group, while these differences did not reach significance in a-MCI group (Fig. 6). No within subject or interaction effects were significant for the other ROIs. For a fair comparison of group effects on normalized hippocampal volume, only subjects that were included in the task ROI analysis were included. A significant group difference with smaller volume in the a-MCI group ($F_{1,102} = 14.6$, $p < 0.001$) was observed, as expected.

3.2.5. Relationship of ROI-based CBF and hippocampal volume with group status

As described above, both hippocampal CBF in the task condition and hippocampal volume displayed similar effect sizes for discriminating between HC and a-MCI patients. However, we were interested in the degree to which they provided complementary information in prediction of disease status. To test this, we developed a two-step, hierarchical

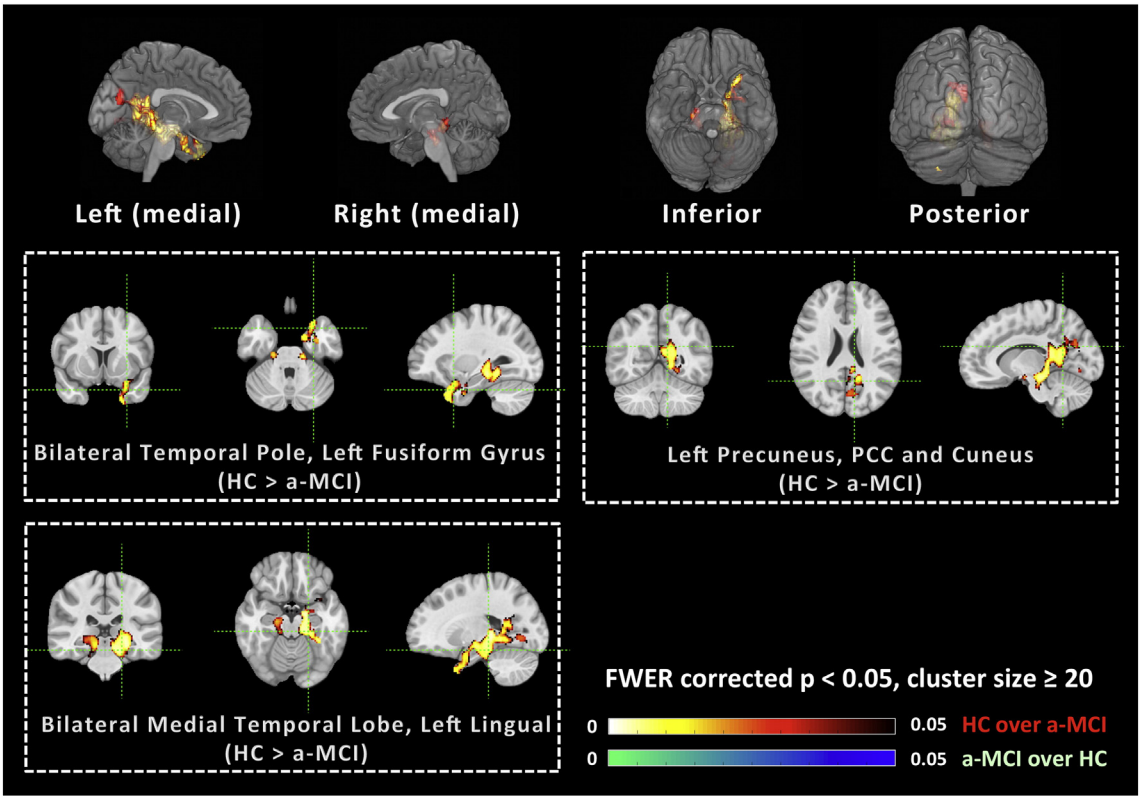

Fig. 3. Between group rCBF difference maps for scene-encoding task after correcting for multiple comparisons using FWER correction. The effects are shown in 3D glass brain (top) and selected slices (bottom).

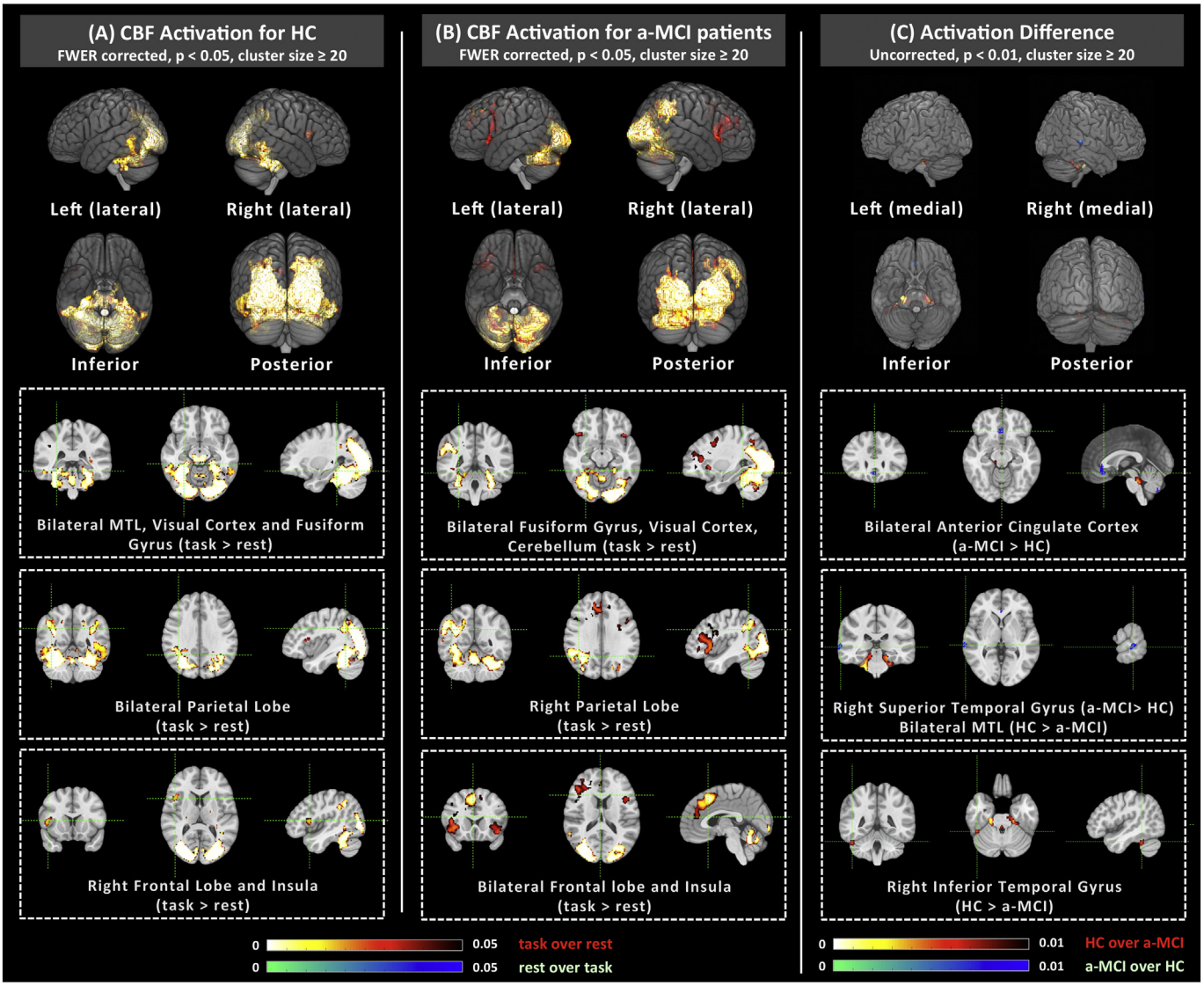

Fig. 4. Scene-encoding task activation (task aCBF — rest aCBF) maps (A) for HC and (B) for a-MCI. (C) Task activation difference between HC and a-MCI groups. The effects are shown in 3D glass brain (top) and selected slices (bottom).

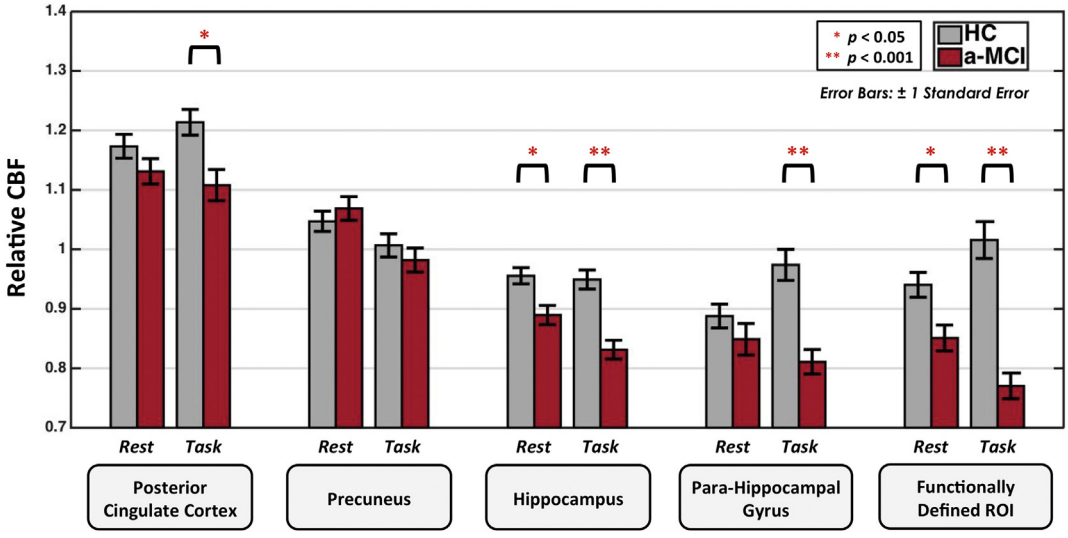

Fig. 5. Comparisons of rest baseline and scene-encoding task ROI rCBF results. ANCOVA was applied to exam the between group effects (using rCBF) for the five ROIs in rest/task condition, with age, gender and education as covariates. Overall, the group differences were stronger when performing scene-encoding task.

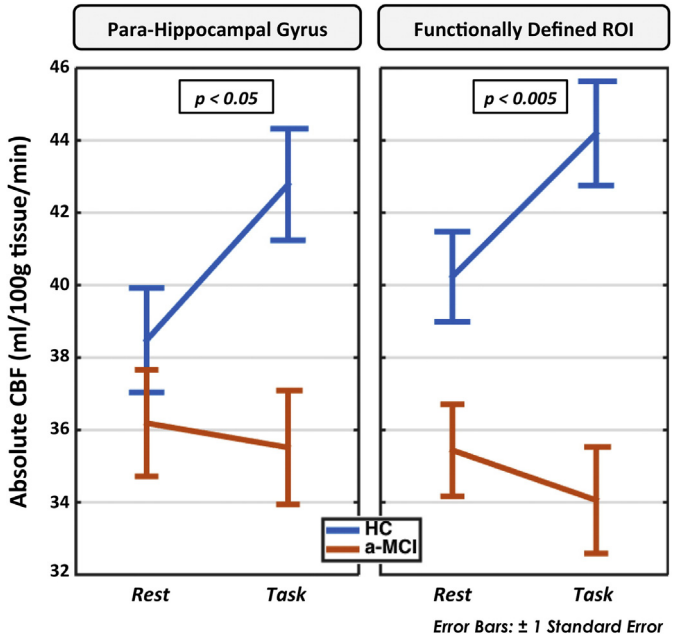

Fig. 6. Interaction effects of groups and conditions on CBF for parahippocampal gyrus and functionally defined ROI. A 2 (groups: HC, a-MCI) × 2 (conditions: rest, task) mixed-effects ANOVA, with age, gender and education as covariates, was applied to look at interaction between group and condition (using aCBF).

logistic regression with age, gender and education entered in the first step and then CBF ROIs at rest and task (PCC, precuneus, hippocampus, and parahippocampal gyrus) and normalized hippocampal volume included in the second step for prediction of group status (HC versus a-MCI). Task hippocampal rCBF ($\beta = -6.4$, $p < 0.005$) and normalized hippocampal volume ($\beta = -0.002$, $p < 0.05$) were included in the model yielding the highest predictive value ($\chi^2_6 = 43.3$, $p < 0.0001$).

4. Discussion

In the current study, both voxel-based and ROI analyses have demonstrated that memory-encoding-task-enhanced ASL MRI increased sensitivity for discriminating a-MCI, memory impaired patients with a relatively high likelihood of developing clinical AD, from HC comparing to rest ASL MRI. Additionally, the results showed that ASL MRI provides explanatory power beyond standard structural MRI biomarker measurement (i.e. hippocampal volume), and the combination of the two has promising potential to be a biomarker for AD. Overall, the rest and task CBF findings are consistent with findings that have previously been reported in the literature.

4.1. Memory encoding task accentuates functional abnormality

Compared to the findings at rest, much stronger group differences were observed during performance of the visual scene memory encoding task in which HC had generally increased rCBF relative to the a-MCI group. Among all the regions, HC had most significantly increased CBF in the MTL relative to a-MCI, which accentuated a weaker effect in this region at rest. ROI analyses further confirmed this finding and demonstrated significant CBF increases in parahippocampal gyrus and the functionally defined ROI in the HC group with, if anything, mild decreases in CBF in the a-MCI group, thus resulting in greater discrimination during the task condition. This result echoes the findings reported by Xu and colleagues, which is the only prior study that has examined the effect of task using ASL MRI in patients with a-MCI (Xu et al., 2007). The Xu et al. study also employed a visual scene memory encoding task, but despite the much smaller sample size (MCI: n = 10; HC: n = 12) and more limited brain coverage of that study, the results were quite similar to that found here. While cognitively normal older adults demonstrated an increase in right parahippocampal gyrus CBF relative to a control condition (22.7%), patients with a-MCI displayed no evidence of increased perfusion during memory encoding. In fact, there was a tendency for decreased CBF (−5.2%) with task. That study did not report resting CBF in the MTL, but a voxel-wise analysis did not find significant differences between the groups at rest in this region. As a general finding and similar to the present data, Xu and colleagues reported that task-related ASL measures appeared to enhance discrimination between the groups relative to rest. Indeed, our task CBF measures produced much more robust group differences than comparisons made at rest. These findings support the idea that ASL MRI acquired during task activation could potentially be implemented as a type of physiologic 'stress test', which might best bring out functional differences in early disease stages.

Both HC and a-MCI displayed regions of increased CBF during performance of the scene-encoding task relative to rest. Indeed, the present findings of increased perfusion in visual association cortex extending into the inferior temporal lobe and MTL, is quite consistent with an earlier ASL study in young adults using this same task (Fernández-Seara et al., 2007). Nonetheless, there were differences in task relative to rest CBF in the two groups studied here. While a-MCI patients displayed evidence of deficient capacity to modulate MTL CBF during memory encoding, they did appear to demonstrate some areas of additional recruitment relative to the HC counterparts. While these findings outside the MTL are more tentative, as they did not survive correction for multiple comparisons, they are consistent with some prior work with BOLD fMRI and PET, which have also reported extra-MTL neocortical areas of increased recruitment in individuals at genetic risk for AD or those with AD (Becker et al., 1996; Bookheimer et al., 2000; Stern et al., 2000; Sperling et al., 2003; Bondi et al., 2005). It has been argued that this additional recruitment may reflect compensatory activation in the service of an inefficient or dysfunctional episodic memory network. Interestingly, anterior cingulate, one of the areas of increased CBF in the a-MCI relative to HC, is a node of the so-called "salience network", which was recently reported to display increased functional connectivity in ε4 carriers in the context of decreased default mode network connectivity (Machulda et al., 2011).

4.2. ASL and structural measurements track disease status

Our ROI analyses demonstrate that the ability of task ASL to discriminate a-MCI from HC is comparable to hippocampal volume measured by T1-weighted structural MRI, which is one of the most well established neuroimaging biomarkers in these populations (Jack et al., 2010). Furthermore, logistic regression analysis suggested that ASL and structural MRI provide complementary information in predicting disease status. This result echoes a recent study by Tosun et al. (2014), which reported that combined structural and CBF MRI measures in early MCI contributed to the best prediction of amyloid status in this population. Further, this group previously demonstrated dissociations between volumetric and CBF alterations dependent on disease stage (Mattsson et al., 2014). Given the ease of acquiring rest, task and structural measurements in the same scanning session (total time here of ~17 min), the combination of these measurements has promising potential utility as a biomarker for monitoring disease course in neurodegenerative conditions for clinical practice and trial use.

4.3. Rest CBF comparisons

While the effects were relative modest both in ROI and voxel-wise comparisons, our findings at rest support the notion that CBF measured by ASL MRI largely recapitulates the pattern of hypometabolism measured by FDG PET in similar populations (Xu et al., 2007; Alsop et al., 2010; Chao et al., 2010; Musiek et al., 2012). Similar to the report of

Dai et al., our a-MCI group also displayed hypoperfusion to the posterior cingulate and precuneus in the voxel-wise analysis. Hypometabolism in these structures is frequently reported as one of the earliest functional alterations seen in AD populations (Petrie et al., 2009; Filippini et al., 2011). Additionally, our finding of relative hypoperfusion in the a-MCI relative to HC in anterior cingulate was also recently reported with ASL MRI (Filippini et al., 2011). Furthermore, consistent with FDG PET studies, which have generally reported hypo- (De Santi et al., 2001; Mevel et al., 2007; Mosconi et al., 2008) or preserved metabolism (Minoshima et al., 1997; Chételat et al., 2008) in MTL in early AD, our a-MCI group also showed lower rest CBF in both voxel-wise and ROI analyses. A similar result was reported in prior ASL studies by Bangen et al. (2012) and Mattsson et al. (2014). However, in the ASL MRI literature a couple of studies have reported the opposite effect, i.e. hyperperfusion in the MTL (Alsop et al., 2008; Dai et al., 2009; Fleisher et al., 2009). The reason for the contradictory results is unclear, but might be due to the complex alternation of MTL perfusion at the course of early disease progression. Hyper-perfusion in MTL may occur at the earliest stage to compensate altered metabolism (Alsop et al., 2008; Dai et al., 2009) followed by hypo-perfusion when the compensatory system fails at the later stages. The findings in the Bangen et al. study (Bangen et al., 2012) might give support to this hypothesis, where they observed hyper-perfusion in cognitively normal apolipoprotein E ε4 carriers, who are individuals at high risk of preclinical AD (Morris et al., 2010), and hypo-perfusion in a-MCI. Alternatively, Mattsson et al. reported relative hypoperfusion in early MCI patients with evidence of amyloid although this result did not reach significance (Mattsson et al., 2014). It is possible the relationship of perfusion changes to early pre-symptomatic and prodromal phases of disease may vary across individuals and cohorts, depending on age, education, and other factors that may alter cognitive reserve. Additionally, a-MCI is generally a heterogeneous group with regard to etiology and this may contribute to contradictory findings in the literature.

5. Conclusions and future work

The current work provides support for the potential utility of ASL MRI as a biomarker for AD, in addition to providing insight into the functional changes associated with memory decline in this population. The enhanced group discrimination associated with task ASL relative to resting ASL supports the general notion that physiologic measures during a cognitive challenge or "stress test" may enhance the ability to detect subtle functional changes in early disease stages. Further, the finding that both ASL and structural MRI provide complementary information of disease status demonstrates the potential of multi-modal MRI-based approaches. Increasingly available background-suppressed ASL MRI pulse sequences (Alsop et al., 2014) should further increase the sensitivity and reliability of this approach, which is readily combined with structural MRI during the same noninvasive imaging session.

The current study has several limitations. a-MCI is a heterogeneous population and use of molecular biomarkers of AD (e.g. CSF Aβ) or longitudinal follow-up to determine who in the group likely was in the prodromal phase of AD would allow for determination of the specificity of the current findings. Additional longitudinal follow-up with recruitment of a larger cohort are planned for future analyses. Also, the interaction of cerebrovascular disease or its risk factors with CBF alterations at rest and during task was not pursued, but is an important area of future enquiry in these populations.

Conflict of interest

Dr. Wolk has received grant funding and consulting fees from GE Healthcare, grant funding from AVID Radiopharmaceuticals, and consulting fees for Piramal Healthcare.

Acknowledgements

This work was supported by the National Institutes of Health (grant numbers R01-AG040271, P30-AG010124, R01-MH080729, R21-DC011074, R03-DA023496, RR02305, R21-DA026114 and R01-DA025906).

References

Alsop, D.C., Detre, J.A., Grossman, M., 2000. Assessment of cerebral blood flow in Alzheimer's disease by spin-labeled magnetic resonance imaging. Ann. Neurol. 47, 93–100.
Alsop, D.C., Casement, M., de Bazelaire, C., Fong, T., Press, D.Z., 2008. Hippocampal hyperperfusion in Alzheimer's disease. NeuroImage 42, 1267–1274.
Alsop, D.C., Dai, W., Grossman, M., Detre, J.A., 2010. Arterial spin labeling blood flow MRI: its role in the early characterization of Alzheimer's disease. J. Alzheimers Dis. 20, 871–880.
Alsop, D.C., Detre, J.A., Golay, X., Günther, M., Hendrikse, J., Hernandez-Garcia, L., Lu, H., Macintosh, B.J., Parkes, L.M., Smits, M., van Osch, M.J.P., Wang, D.J.J., Wong, E.C., Zaharchuk, G., 2014. Recommended implementation of arterial spin-labeled perfusion MRI for clinical applications: a consensus of the ISMRM perfusion study group and the European consortium for ASL in dementia. Magn. Reson. Med. 73, 102–116.
Attwell, D., Laughlin, S.B., 2001. An energy budget for signaling in the grey matter of the brain. J. Cereb. Blood Flow Metab. 21, 1133–1145.
Avants, B.B., Epstein, C.L., Grossman, M., Gee, J.C., 2008. Symmetric diffeomorphic image registration with cross-correlation: evaluating automated labeling of elderly and neurodegenerative brain. Med. Image Anal. 12, 26–41.
Bangen, K.J., Restom, K., Liu, T.T., Wierenga, C.E., Jak, A.J., Salmon, D.P., Bondi, M.W., 2012. Assessment of Alzheimer's disease risk with functional magnetic resonance imaging: an arterial spin labeling study. J. Alzheimers Dis. 31 (Suppl. 3), S59–S74.
Becker, J.T., Mintun, M.A., Aleva, K., Wiseman, M.B., Nichols, T., DeKosky, S.T., 1996. Compensatory reallocation of brain resources supporting verbal episodic memory in Alzheimer's disease. Neurology 46, 692–700.
Bondi, M.W., Houston, W.S., Eyler, L.T., Brown, G.G., 2005. fMRI evidence of compensatory mechanisms in older adults at genetic risk for Alzheimer disease. Neurology 64, 501–508.
Bookheimer, S.Y., Strojwas, M.H., Cohen, M.S., Saunders, A.M., Pericak-Vance, M.A., Mazziotta, J.C., Small, G.W., 2000. Patterns of brain activation in people at risk for Alzheimer's disease. N. Engl. J. Med. 343, 450–456.
Chao, L.L., Pa, J., Duarte, A., Schuff, N., Weiner, M.W., Kramer, J.H., Miller, B.L., Freeman, K.M., Johnson, J.K., 2009. Patterns of cerebral hypoperfusion in amnestic and dysexecutive MCI. Alzheimer Dis. Assoc. Disord. 23, 245–252.
Chao, L.L., Buckley, S.T., Kornak, J., Schuff, N., Madison, C., Yaffe, K., Miller, B.L., Kramer, J.H., Weiner, M.W., 2010. ASL perfusion MRI predicts cognitive decline and conversion from MCI to dementia. Alzheimer Dis. Assoc. Disord. 24, 19–27.
Chen, Y., Wang, J., Korczykowski, M., Fernandez-Seara, M., Detre, J., 2010. Comparison of reproducibility between continuous, pulsed, and pseudo-continuous arterial spin labeling. Proc. Int. Soc. Magn. Reson. Med. 18, 4078.
Chen, Y., Wolk D, A., Reddin, J.S., Korczykowski, M., Martinez, P.M., Musiek, E.S., Newberg, A.B., Julin, P., Arnold, S.E., Greenberg, J.H., Detre J, A., 2011. Voxel-level comparison of arterial spin-labeled perfusion MRI and FDG-PET in Alzheimer disease. Neurology 77, 1977–1985.
Chételat, G., Desgranges, B., Landeau, B., Mézenge, F., Poline, J.B., de la Sayette, V., Viader, F., Eustache, F., Baron, J.-C., 2008. Direct voxel-based comparison between grey matter hypometabolism and atrophy in Alzheimer's disease. Brain 131, 60–71.
Dai, W., Garcia, D., de Bazelaire, C., Alsop, D.C., 2008. Continuous flow-driven inversion for arterial spin labeling using pulsed radio frequency and gradient fields. Magn. Reson. Med. 60, 1488–1497.
Dai, W., Lopez, O.L., Carmichael, O.T., Becker, J.T., Kuller, L.H., Gach, H.M., 2009. Mild cognitive impairment and alzheimer disease: patterns of altered cerebral blood flow at MR imaging. Radiology 250, 856–866.
Das, S.R., Pluta, J., Mancuso, L., Kliot, D., Orozco, S., Dickerson, B.C., Yushkevich, P.A., Wolk D, A., 2013. Increased functional connectivity within medial temporal lobe in mild cognitive impairment. Hippocampus 23, 1–6.
De Santi, S., de Leon, M.J., Rusinek, H., Convit, A., Tarshish, C.Y., Roche, A., Tsui, W.H., Kandil, E., Boppana, M., Daisley, K., Wang, G.J., Schlyer, D., Fowler, J., 2001. Hippocampal formation glucose metabolism and volume losses in MCI and AD. Neurobiol. Aging 22, 529–539.
Dickerson, B.C., Sperling, R.A., 2009. Large-scale functional brain network abnormalities in Alzheimer's disease: insights from functional neuroimaging. Behav. Neurol. 21, 63–75.
Engler, H., Forsberg, A., Almkvist, O., Blomquist, G., Larsson, E., Savitcheva, I., Wall, A., Ringheim, A., Långström, B., Nordberg, A., 2006. Two-year follow-up of amyloid deposition in patients with Alzheimer's disease. Brain 129, 2856–2866.
Fernández-Seara, M.A., Wang, J., Wang, Z., Korczykowski, M., Guenther, M., Feinberg, D.A., Detre, J.A., 2007. Imaging mesial temporal lobe activation during scene encoding: comparison of fMRI using BOLD and arterial spin labeling. Hum. Brain Mapp. 28, 1391–1400.
Filippini, N., Ebmeier, K.P., MacIntosh, B.J., Trachtenberg, A.J., Frisoni, G.B., Wilcock, G.K., Beckmann, C.F., Smith, S.M., Matthews, P.M., Mackay, C.E., 2011. Differential effects of the APOE genotype on brain function across the lifespan. NeuroImage 54, 602–610.
Fleisher, A.S., Podraza, K.M., Bangen, K.J., Taylor, C., Sherzai, A., Sidhar, K., Liu, T.T., Dale, A.M., Buxton, R.B., 2009. Cerebral perfusion and oxygenation differences in Alzheimer's disease risk. Neurobiol. Aging 30, 1737–1748.

Folstein, M.F., Folstein, S.E., McHugh, P.R., 1975. Mini-mental state. J. Psychiatr. Res. 12, 189–198.
Hu, W.T., Wang, Z., Lee, V.M.-Y., Trojanowski, J.Q., Detre, J.A., Grossman, M., 2010. Distinct cerebral perfusion patterns in FTLD and AD. Neurology 75, 881–888.
Jack, C.R., Lowe, V.J., Senjem, M.L., Weigand, S.D., Kemp, B.J., Shiung, M.M., Knopman, D.S., Boeve, B.F., Klunk, W.E., Mathis, C.A., Petersen, R.C., 2008. 11C PiB and structural MRI provide complementary information in imaging of Alzheimer's disease and amnestic mild cognitive impairment. Brain 131, 665–680.
Jack, C.R., Lowe, V.J., Weigand, S.D., Wiste, H.J., Senjem, M.L., Knopman, D.S., Shiung, M.M., Gunter, J.L., Boeve, B.F., Kemp, B.J., Weiner, M., Petersen, R.C., 2009. Serial PIB and MRI in normal, mild cognitive impairment and Alzheimer's disease: implications for sequence of pathological events in Alzheimer's disease. Brain 132, 1355–1365.
Jack, C.R., Knopman, D.S., Jagust, W.J., Shaw, L.M., Aisen, P.S., Weiner, M.W., Petersen, R.C., Trojanowski, J.Q., 2010. Hypothetical model of dynamic biomarkers of the Alzheimer's pathological cascade. Lancet Neurol. 9, 119–128.
Jagust, W.J., Landau, S.M., Shaw, L.M., Trojanowski, J.Q., Koeppe, R.A., Reiman, E.M., Foster, N.L., Petersen, R.C., Weiner, M.W., Price, J.C., Mathis, C.A., 2009. Relationships between biomarkers in aging and dementia. Neurology 73, 1193–1199.
Jagust, W.J., Bandy, D., Chen, K., Foster, N.L., Landau, S.M., Mathis, C.A., Price, J.C., Reiman, E.M., Skovronsky, D., Koeppe, R.A., 2010. The Alzheimer's Disease Neuroimaging Initiative positron emission tomography core. Alzheimers Dement. 6, 221–229.
Kaplan, E., Goodglass, H., Weintraub, S., 1983. The Boston Naming Test. second ed. Lea & Febiger, Philadelphia.
Machulda, M.M., Jones, D.T., Vemuri, P., McDade, E., Avula, R., Przybelski, S., Boeve, B.F., Knopman, D.S., Petersen, R.C., Jack, C.R., 2011. Effect of APOE ε4 status on intrinsic network connectivity in cognitively normal elderly subjects. Arch. Neurol. 68, 1131–1136.
Mattsson, N., Tosun, D., Insel, P.S., Simonson, A., Jack, C.R., Beckett, L.A., Donohue, M., Jagust, W., Schuff, N., MW, Weiner, 2014. Association of brain amyloid-β with cerebral perfusion and structure in Alzheimer's disease and mild cognitive impairment. Brain 137, 1550–1561.
Mechanic-Hamilton, D., Korczykowski, M., Yushkevich, P.A., Lawler, K., Pluta, J., Glynn, S., Tracy, J.I., Wolf, R.L., Sperling, M.R., French, J.A., Detre, J.A., 2009. Hippocampal volumetry and functional MRI of memory in temporal lobe epilepsy. Epilepsy Behav. 16, 128–138.
Mevel, K., Desgranges, B., Baron, J.-C., Landeau, B., De la Sayette, V., Viader, F., Eustache, F., Chételat, G., 2007. Detecting hippocampal hypometabolism in Mild Cognitive Impairment using automatic voxel-based approaches. NeuroImage 37, 18–25.
Minoshima, S., Giordani, B., Berent, S., Frey, K.A., Foster, N.L., Kuhl, D.E., 1997. Metabolic reduction in the posterior cingulate cortex in very early Alzheimer's disease. Ann. Neurol. 42, 85–94.
Morris, J.C., Heyman, A., Mohs, R.C., Hughes, J.P., van Belle, G., Fillenbaum, G., Mellits, E.D., Clark, C., 1989. The Consortium to Establish a Registry for Alzheimer's Disease (CERAD). Part I. Clinical and neuropsychological assessment of Alzheimer's disease. Neurology 39, 1159–1165.
Morris, J.C., Roe, C.M., Xiong, C., Fagan, A.M., Goate, A.M., Holtzman, D.M., Mintun, M.A., 2010. APOE predicts amyloid-beta but not tau Alzheimer pathology in cognitively normal aging. Ann. Neurol. 67, 122–131.
Mosconi, L., De Santi, S., Li, J., Tsui, W.H., Li, Y., Boppana, M., Laska, E., Rusinek, H., de Leon, M.J., 2008. Hippocampal hypometabolism predicts cognitive decline from normal aging. Neurobiol. Aging 29, 676–692.
Mugler, J.P., Brookeman, J.R., 1990. Three-dimensional magnetization-prepared rapid gradient-echo imaging (3D MP RAGE). Magn. Reson. Med. 15, 152–157.
Musiek, E.S., Chen, Y., Korczykowski, M., Saboury, B., Martinez, P.M., Reddin, J.S., Alavi, A., Kimberg, D.Y., Wolk, D.A., Julin, P., Newberg, A.B., Arnold, S.E., Detre, J.A., 2012. Direct comparison of fluorodeoxyglucose positron emission tomography and arterial spin labeling magnetic resonance imaging in Alzheimer's disease. Alzheimers Dement. 8, 51–59.
Petersen, R.C., 2004. Mild cognitive impairment as a diagnostic entity. J. Intern. Med. 256, 183–194.
Petersen, R.C., Roberts, R.O., Knopman, D.S., Boeve, B.F., Geda, Y.E., Ivnik, R.J., Smith, G.E., Jack, C.R., 2009. Mild cognitive impairment: ten years later. Arch. Neurol. 66, 1447–1455.
Petrie, E.C., Cross, D.J., Galasko, D., Schellenberg, G.D., Raskind, M.A., Peskind, E.R., Minoshima, S., 2009. Preclinical evidence of Alzheimer changes: convergent cerebrospinal fluid biomarker and fluorodeoxyglucose positron emission tomography findings. Arch. Neurol. 66, 632–637.
Raichle, M.E., 1998. Behind the scenes of functional brain imaging: a historical and physiological perspective. Proc. Natl. Acad. Sci. 95, 765–772.
Reitan, R.M., 1958. Validity of the trail making test as an indicator of organic brain damage. Percept. Mot. Skills 8, 271–276.
Schwartz, W., Smith, C., Davidsen, L., Savaki, H., Sokoloff, L., Mata, M., Fink, D., Gainer, H., 1979. Metabolic mapping of functional activity in the hypothalamo-neurohypophysial system of the rat. Science 80- (205), 723–725.
Smith, S.M., Nichols, T.E., 2009. Threshold-free cluster enhancement: addressing problems of smoothing, threshold dependence and localisation in cluster inference. NeuroImage 44, 83–98.
Snodgrass, J.G., Corwin, J., 1988. Pragmatics of measuring recognition memory: applications to dementia and amnesia. J. Exp. Psychol. Gen. 117, 34–50.
Sperling, R.A., Bates, J.F., Chua, E.F., Cocchiarella, A.J., Rentz, D.M., Rosen, B.R., Schacter, D.L., Albert, M.S., 2003. fMRI studies of associative encoding in young and elderly controls and mild Alzheimer's disease. J. Neurol. Neurosurg. Psychiatry 74, 44–50.
Spreen, O., Strauss, E., 1998. A compendium of neuropsychological tests: administration, norms, and commentary.
Stark, C.E., Squire, L.R., 2001. When zero is not zero: the problem of ambiguous baseline conditions in fMRI. Proc. Natl. Acad. Sci. U. S. A. 98, 12760–12766.
Stern, Y., Moeller, J.R., Anderson, K.E., Luber, B., Zubin, N.R., DiMauro, A.A., Park, A., Campbell, C.E., Marder, K., Bell, K., Van Heertum, R., Sackeim, H.A., 2000. Different brain networks mediate task performance in normal aging and AD: defining compensation. Neurology 55, 1291–1297.
Terry, R.D., Masliah, E., Salmon, D.P., Butters, N., DeTeresa, R., Hill, R., Hansen, L.A., Katzman, R., 1991. Physical basis of cognitive alterations in Alzheimer's disease: synapse loss is the major correlate of cognitive impairment. Ann. Neurol. 30, 572–580.
Thies, W., Bleiler, L., 2013. 2013 Alzheimer's disease facts and figures. Alzheimers Dement. 9, 208–245.
Tosun, D., Joshi, S., Weiner, M.W., 2014. Multimodal MRI-based Imputation of the Aβ+ in Early Mild Cognitive Impairment. Ann. Clin. Transl. Neurol. 1, 160–170.
Tzourio-Mazoyer, N., Landeau, B., Papathanassiou, D., Crivello, F., Etard, O., Delcroix, N., Mazoyer, B., Joliot, M., 2002. Automated anatomical labeling of activations in SPM using a macroscopic anatomical parcellation of the MNI MRI single-subject brain. NeuroImage 15, 273–289.
Vemuri, P., Wiste, H.J., Weigand, S.D., Shaw, L.M., Trojanowski, J.Q., Weiner, M.W., Knopman, D.S., Petersen, R.C., Jack, C.R., 2009a. MRI and CSF biomarkers in normal, MCI, and AD subjects: predicting future clinical change. Neurology 73, 294–301.
Vemuri, P., Wiste, H.J., Weigand, S.D., Shaw, L.M., Trojanowski, J.Q., Weiner, M.W., Knopman, D.S., Petersen, R.C., Jack, C.R., 2009b. MRI and CSF biomarkers in normal, MCI, and AD subjects: diagnostic discrimination and cognitive correlations. Neurology 73, 287–293.
Walsh, D.M., Selkoe, D.J., 2004. Deciphering the molecular basis of memory failure in Alzheimer's disease. Neuron 44, 181–193.
Wang, J., Alsop, D.C., Song, H.K., Maldjian, J.A., Tang, K., Salvucci, A.E., Detre J, A., 2003. Arterial transit time imaging with flow encoding arterial spin tagging (FEAST). Magn. Reson. Med. 50, 599–607.
Wang, Z., Aguirre, G.K., Rao, H., Wang, J., Fernández-Seara, M.A., Childress, A.R., Detre, J.A., 2008. Empirical optimization of ASL data analysis using an ASL data processing toolbox: ASLtbx. Magn. Reson. Imaging 26, 261–269.
Wang, H., Suh, J.W., Das, S.R., Pluta, J., Craige, C., Yushkevich, P.A., 2012. Multi-Atlas segmentation with joint label fusion. IEEE Trans. Pattern Anal. Mach. Intell. 35, 611–623.
Wang, Z., Das, S.R., Xie, S.X., Arnold, S.E., Detre, J.A., Wolk, D.A., 2013. Arterial spin labeled MRI in prodromal Alzheimer's disease: a multi-site study. NeuroImage Clin. 2, 630–636.
Wechsler, D., 1987. Wechsler Memory Scale-Revised Manual. San Antonio, TX, U.S.A..
Winblad, B., Palmer, K., Kivipelto, M., Jelic, V., Fratiglioni, L., Wahlund, L.-O., Nordberg, A., Bäckman, L., Albert, M., Almkvist, O., Arai, H., Basun, H., Blennow, K., de Leon, M., DeCarli, C., Erkinjuntti, T., Giacobini, E., Graff, C., Hardy, J., Jack, C., Jorm, A., Ritchie, K., van Duijn, C., Visser, P., Petersen, R.C., 2004. Mild cognitive impairment–beyond controversies, towards a consensus: report of the International Working Group on Mild Cognitive Impairment. J. Intern. Med. 256, 240–246.
Winkler, A.M., Ridgway, G.R., Webster, M.A., Smith, S.M., Nichols, T.E., 2014. Permutation inference for the general linear model. NeuroImage 92, 381–397.
Wu, W.-C., Fernández-Seara, M., Detre, J.A., Wehrli, F.W., Wang, J., 2007. A theoretical and experimental investigation of the tagging efficiency of pseudocontinuous arterial spin labeling. Magn. Reson. Med. 58, 1020–1027.
Wu, W.-C., Edlow, B.L., Elliot, M.A., Wang, J., Detre, J.A., 2009. Physiological modulations in arterial spin labeling perfusion magnetic resonance imaging. IEEE Trans. Med. Imaging 28, 703–709.
Xu, G., Antuono, P.G., Jones, J., Xu, Y., Wu, G., Ward, D., Li, S.-J., 2007. Perfusion fMRI detects deficits in regional CBF during memory-encoding tasks in MCI subjects. Neurology 69, 1650–1656.
Xu, G., Rowley, H.A., Wu, G., Alsop, D.C., Shankaranarayanan, A., Dowling, M., Christian, B.T., Oakes, T.R., Johnson, S.C., 2010. Reliability and precision of pseudo-continuous arterial spin labeling perfusion MRI on 3.0 T and comparison with 15O-water PET in elderly subjects at risk for Alzheimer's disease. NMR Biomed. 23, 286–293.
Yassa, M.A., Stark, S.M., Bakker, A., Albert, M.S., Gallagher, M., Stark, C.E.L., 2010. High-resolution structural and functional MRI of hippocampal CA3 and dentate gyrus in patients with amnestic Mild Cognitive Impairment. NeuroImage 51, 1242–1252.
Ye, F.Q., Berman, K.F., Ellmore, T., Esposito, G., van Horn, J.D., Yang, Y., Duyn, J., Smith, A.M., Frank, J.A., Weinberger, D.R., McLaughlin, A.C., 2000. H(2)(15)O PET validation of steady-state arterial spin tagging cerebral blood flow measurements in humans. Magn. Reson. Med. 44, 450–456.
Yoshiura, T., Hiwatashi, A., Yamashita, K., Ohyagi, Y., Monji, A., Takayama, Y., Nagao, E., Kamano, H., Noguchi, T., Honda, H., 2009. Simultaneous measurement of arterial transit time, arterial blood volume, and cerebral blood flow using arterial spin-labeling in patients with Alzheimer disease. AJNR Am. J. Neuroradiol. 30, 1388–1393.
Yushkevich, P.A., Piven, J., Hazlett, H.C., Smith, R.G., Ho, S., Gee, J.C., Gerig, G., 2006. User-guided 3D active contour segmentation of anatomical structures: significantly improved efficiency and reliability. NeuroImage 31, 1116–1128.
Zhang, Y., Schuff, N., Ching, C., Tosun, D., Zhan, W., Nezamzadeh, M., Rosen, H.J., Kramer, J.H., Gorno-Tempini, M.L., Miller, B.L., Michael, W.W., 2011. Joint assessment of structural, perfusion, and diffusion MRI in Alzheimer's disease and frontotemporal dementia. Int. J. Alzheimers Dis. 2011.
Zhang, K., Herzog, H., Mauler, J., Filss, C., Okell, T.W., Kops, E.R., Tellmann, L., Fischer, T., Brocke, B., Sturm, W., Coenen, H.H., Shah, N.J., 2014. Comparison of cerebral blood flow acquired by simultaneous [15O] water positron emission tomography and arterial spin labeling magnetic resonance imaging. J. Cereb. Blood Flow Metab. 34, 1373–1380.